

## Discovery of 20 UV Emitting SNRs in M31 with UVIT

DENIS LEAHY,<sup>1</sup> CHRISTOPHER MONAGHAN,<sup>1</sup> AND SUJITH RANASINGHE<sup>1</sup>

<sup>1</sup>*Dept. Physics and Astronomy, University of Calgary, Calgary, AB, Canada;*

(Received; Revised; Accepted January 26, 2023)

Submitted to AJ

### ABSTRACT

We present the first catalog of supernova remnants (SNRs) in M31 which exhibit diffuse ultraviolet (UV) emission. UV images of M31 were obtained by the Ultraviolet Imaging Telescope (UVIT) on the AstroSat satellite, and the list of SNRs was obtained from X-ray, optical and radio catalogues of SNRs in M31. We used the UVIT images to find SNRs with diffuse emission, omitting those too contaminated with stellar emission. 20 SNRs in M31 were detected with diffuse UV emission. Fluxes in the UVIT F148W, F169M, F172M, N219M and N279N filters are measured for these SNRs. The luminosities are compared to those computed from the spectra of seven known UV-emitting SNRs in the Milky Way, the LMC, and the SMC. We find similar spectral shapes between the known and the M31 UV-emitting SNRs. The spectral shapes and the diffuse nature of the emission are good evidence that the UV emissions are dominated by line emissions, like known SNRs, and the UV is associated with the SNRs. Models are applied to the 6 SNRs with X-ray spectra. The main difference is that the 2 X-ray/UV SNRs are Type Ia and the 4 X-ray/non-UV SNRs are core-collapse or unknown type. A comparison of M31 SNRs in different wavebands shows that most are detected optically, similar to the case for other nearby galaxies. 19 of the 20 UV-emitting SNRs are detected optically, expected because both UV and optical are from forbidden and recombination lines from shock-ionized gas.

*Keywords:* Andromeda Galaxy (39); Ultraviolet astronomy(1736); Supernova remnants()

### 1. INTRODUCTION

A supernova remnant (SNR) is an extended (pc scale) structure in the interstellar medium excited by the shock wave from the explosive death of a star at the end of its life. The study of SNRs is crucial to our understanding of supernova explosions, the nature of shock waves and the structure of the interstellar medium. SNRs emit over a wide range of wavelengths, thus Galactic and extragalactic surveys of SNRs have been conducted at optical, radio, and X-ray wavelengths. There are 294 known SNRs within the Milky Way (Green 2019). A small number of nearby external galaxies have had their SNRs catalogued, including the Large and Small Magellanic Clouds (LMC & SMC), M33, NGC 300 and M31. E.g. there are 62 confirmed SNRs and 30 SNR candidates in the LMC, and 21 SNRs and 2 candidates in the SMC (Yew et al. 2021; Maggi et al. 2019). There are 109 SNRs and SNR candidates in M33 (Duric 2000; Pannuti et al. 2000) and 44 in NGC 300 (Pannuti et al. 2000). Optical surveys of M31 have found 156 SNRs (Lee & Lee 2014) and XMM-Newton X-ray found 26 SNRs and 21 SNR candidates (Sasaki et al. 2012). Radio emission was found for 30 SNRs in M31 by Braun & Walterbos (1993).

Galactic and extragalactic searches for SNRs have been carried out at optical, radio, and X-ray wavelengths. However, ultraviolet (UV) observations of SNRs are scarce. The difficulty in detecting UV emission is caused by the strong interstellar extinction for our Galaxy in the UV (e.g. Sun et al. 2021). As a result, only nearby Galactic SNRs

have detected UV radiation. However, UV emission lines from SNRs can provide valuable information on the SNR, including shock velocities, densities, and thermal structure (Raymond et al. 1997).

The first major steps in analyzing the UV emission of SNRs came from the International Ultraviolet Explorer (IUE), designed for analyzing UV spectra. IUE data provided the groundwork for the first UV-based analyses of SNRs throughout the 1980's. Many studies focused on comparing theoretical models of shockwaves to nearby SNRs, such as Vela and the Cygnus Loop, by analyzing the individual line emissions in the UV spectrum (Raymond et al. 1980, 1981, 1988). SNRs in the Large Magellanic Cloud and the Small Magellanic Cloud, such as N49, N63, and E0102, were also analyzed using their UV spectra (Benvenuti et al. 1980; Vancura et al. 1992; Benvenuti et al. 1980). Despite the large distances to these sources, their positions with respect to the plane of the Milky Way allows light from the LMC and SMC to pass through less of the interstellar medium, and experience less extinction than most Galactic SNRs. Such studies determined that the UV spectra of these remnants are dominated by line emission, with many of the same lines present in different SNRs. N[V], Si[IV], O[IV], He[II], and O[III] emission lines were observed in more than six intergalactic and extragalactic (LMC and SMC) SNRs, and a number of other lines were identified in more than one SNR (Fesen & Hurford 1996).

Despite the progress in UV-based SNR research, there does not yet exist a catalogue of extragalactic UV-emitting SNRs. As an important step in UV studies of SNRs, we conduct a search for SNRs in M31 using data from AstroSat's UVIT instrument, and generate the first catalog of UV SNRs in another galaxy. Section 2 below summarizes the observations and Section 3 describes our data analysis. In Section 4.1 the catalog of UV-emitting SNRs in M31 is given, and in Section 4.2 the UV spectral shapes of known UV-emitting SNRs are compared to those of the M31 SNRs. The set of 6 SNRs with X-ray spectra are fit with SNR models to derive their physical conditions in Section 4.3. The statistics of numbers of SNRs detected in different wavebands is discussed in Section 4.4 and Section 5 summarized the results from this study.

## 2. OBSERVATIONS

The observations of M31 were carried out by the Ultraviolet Imaging Telescope (UVIT) onboard the AstroSat (Singh et al. 2014). UVIT is capable of observing in a variety of Far Ultraviolet (FUV) and Near Ultraviolet (NUV) bandpasses. The M31 survey includes data with the filters: F148W, F154W, F169M, F172M, N219M, and N279N filters, although the F154W filter was used only for one observation. The filter parameters, including effective area curves, can be found in Tandon et al. (2017). New in-orbit calibrations of UVIT were carried out by Tandon et al. (2020). Data processing was carried out using CCDLab (Postma & Leahy 2017, 2021) to produce images with a pixel scale of  $0.4168'' \times 0.4168''$  from the instrument data. The resulting spatial resolution, using the latest UVIT calibrations and data processing procedure, is  $\simeq 1''$ .

The M31 survey with UVIT (Leahy et al. 2020) consists of 19 partially-overlapping fields, each with a diameter of  $\approx 28'$ , covering a sky area of  $\approx 3.3^\circ \times 1.3^\circ$ . Since the survey paper (Leahy et al. 2020), additional observations were carried out, including observation of the missing field number 8 in F148W and F169M bands to yield full coverage of the M31 survey area in the F148W filter, and partial coverage in the other filters. The images of these 19 fields, each with 2 to 5 filter bands, were used in the analysis carried out here.

## 3. DATA ANALYSIS

### 3.1. Selection of SNRs

The list of SNRs and SNR candidates within M31 was obtained from existing optical, X-ray and radio SNR lists<sup>1</sup>. The optical SNRs were from Lee & Lee (2014), which contained 156 SNR candidates observed using H $\alpha$  and S[II] images. The X-ray SNRs were from Sasaki et al. (2012) which lists 26 confirmed SNRs and 21 SNR candidates. These sources were first catalogued in an XMM-Newton survey of M31, which catalogued a total of 1897 X-ray sources (Stiele et al. 2011). The radio SNRs were from Braun & Walterbos (1993) which lists 24 high confidence ( $> 5\sigma$ ) and 6 medium confidence (3 to  $5\sigma$ ) detections at 1465 MHz. That work found 52 SNRs and candidates using narrow band imaging in [SII] and H $\alpha$  filters of the NE half of M31, then matched those with radio continuum imaging of M31.

We combine the three sets of SNRs. The 52 optically-detected SNRs (including 30 with radio emission) from Braun & Walterbos (1993) were included in the study of Lee & Lee (2014). Four of the 30 with radio emission were re-examined

<sup>1</sup> Galvin & Filipovic (2014) gives a catalog of 916 radio sources in M31 detected at 20cm, however the sources which are SNRs are not identified.

by Lee & Lee (2014) and found not to be SNRs, and one more was found by us to be contaminated by stellar emission. This left 25 SNRs from Braun & Walterbos (1993) that are detected in radio, which are included in the list in Lee & Lee (2014). Some SNRs are listed in both optical and X-ray catalogues as noted in the analysis of X-ray SNRs in the northern disc of the M31 (Sasaki et al. 2018). Using an angular separation of  $18''$ , we found an additional 18 source matches between the radio and X-ray SNR catalogs. This left 179 unique SNRs or SNR candidates, hereafter referred to as SNRs, within M31. However, two of these are outside the M31 UVIT survey region, leaving 177 unique sources for analysis using UVIT data: 119 detected only in optical, 22 detected only in X-ray, 13 detected in optical and radio, 11 detected in optical and X-ray, and 12 detected in optical, X-ray and radio. The location of these 177 SNRs in M31 for the different categories is shown in Figure 1(b).

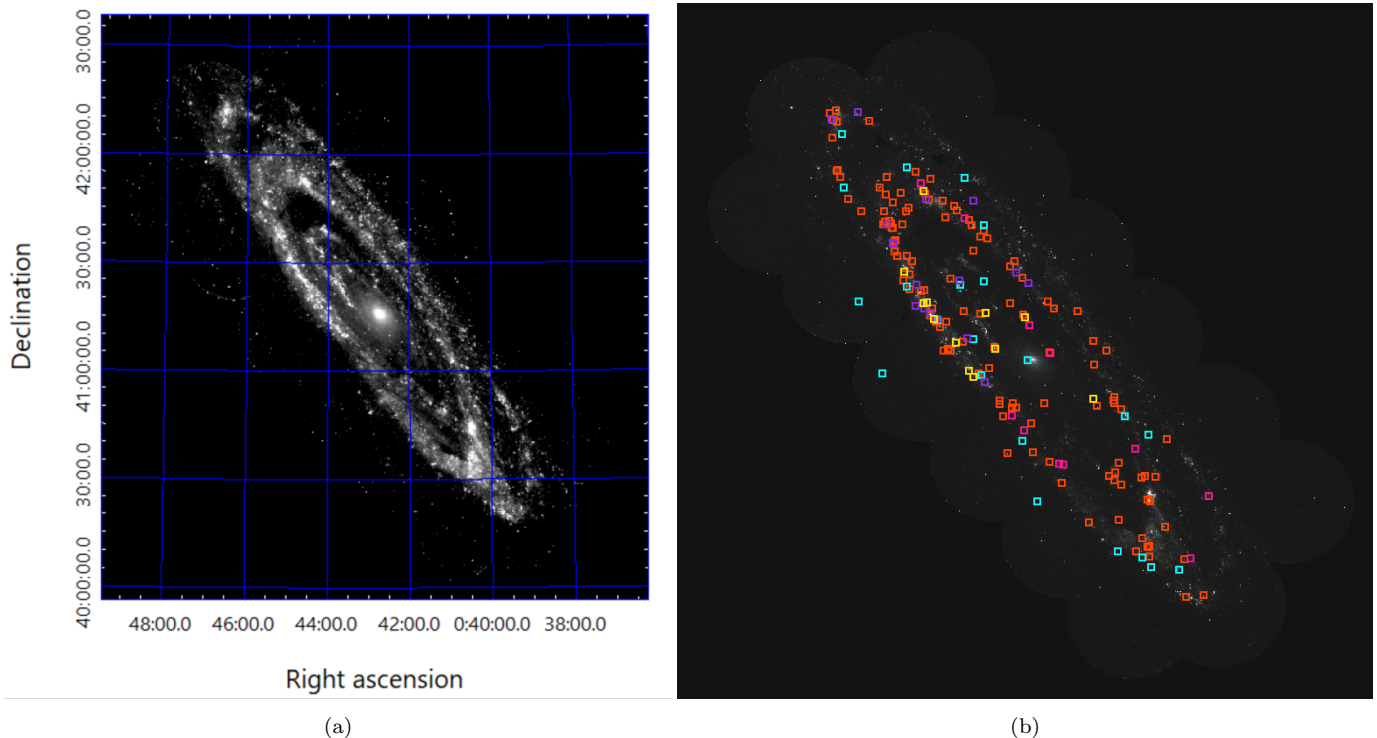


**Figure 1.** (a): the F148W mosaic of M31 (from Leahy et al. 2020) but with missing field 8 added. (b): positions of the 177 SNRs from Lee & Lee (2014) and Sasaki et al. (2012), overlaid on the mosaic (with the mosaic made fainter to clearly see the SNRs). Red squares indicate the positions of SNRs detected in optical, aqua indicates SNRs detected in X-ray, purple indicates SNRs detected in optical and radio, pink indicates SNRs detected in optical and X-ray, and yellow indicates SNRs detected in optical, radio and X-ray. SNRs identified in optical, X-ray and radio in panel (b) closely trace the positions of the spiral arms and star formation which are bright in the F148W image of M31 (panel (a)).

### 3.2. Search for UV emission from the SNRs

The locations of the 177 SNRs were used to determine within which field each object was located and thus which filters were observed for each SNR. Next, we carried out a set of tasks to find those SNRs which have diffuse emission not too contaminated by UV emitting stars in M31. SNRs in UV are characterized by diffuse emission, in contrast to stars which are unresolved point sources. UVIT has high enough spatial resolution in most cases to separate diffuse from the stellar point-source emission.

An initial inspection of the 177 SNRs was undertaken to remove any sources from the list without any UV emission within the optical radius of the SNR, given in Lee & Lee (2014). For the 22 X-ray-only SNRs, no optical SNR radius was available, and neither was an X-ray radius, so the position error was used instead. The radius of analysis around each source (whether from optical or X-ray) is henceforth referred to as the “SNR radius”. Several SNRs were

contained within densely packed, UV-emitting star clusters, so that no SNR emission could be distinguished from the stellar emission. The “no emission” and crowded sources were removed from the list of SNRs for analysis, leaving 126.

Further inspection of these 126 SNRs often revealed stars within the radii of the SNRs. Thus, we search for known stars within the SNR radius of each SNR: Vizier (<https://vizier.cds.unistra.fr/>) was used to search through stellar catalogues. A number of stellar catalogues were initially searched, but most were contained within the GAIA Early Data Release 3 (EDR3) catalogue (Bailer-Jones et al. 2021). We found all EDR3 stars within a 15'' search radius (15'' was the largest optical radius of any source). A total of 766 stars were found in the EDR3 data (many would not have UV emission), and their coordinates were imported into CCDLAB to search for stellar contamination. 42 sources were removed from our SNR list because all UV emission within the SNR radius was identified with catalogued GAIA stars, leaving 84 sources in our list of SNRs. This process was repeated using the full data release (DR3) upon its publication on June 13th, 2022. 5 additional stars were determined to be nearby the SNRs, but none associated with the remaining 84 with UV emission.

The 84 sources were further analyzed by searching for stellar sources from additional stellar catalogues. A number of catalogues were searched during this process, including a BVRI analysis of M31 objects using the McGraw Hill Telescope, a Swift/UVOT source catalogue, and a XMM-OM object survey (Magnier et al. 1992; Yershov 2014; Page et al. 2012). Vizier searches from these catalogues did not provide additional stellar contaminants in the 84 SNRs. However, the catalogue of M31 supergiants from the local group galaxy survey (Massey et al. 2016) provided additional stellar sources within a 15'' search radius of the 84 SNRs. The red supergiant catalogue of Massey et al. (2021) was also included in the Vizier search. 610 supergiants from these two catalogues were found to be nearby our remaining SNRs: most of these were blue supergiants or luminous blue variables. This process led to a number of UV emissions to be reclassified as supergiant stars. 43 sources were removed from our SNR list, leaving 41 SNRs. One more source was removed using the HST M31 PHAT catalogue (Williams et al. 2014) using PHAT stars with F275W magnitude brighter than 20.

Out of the 40 SNRs that remained, 7 had UV emission with no associations with stars. The other 33 consisted of either i) sources with diffuse emissions that overlapped with GAIA stars or Massey supergiants or ii) diffuse emission too dim to be reliably measured. Stars within diffuse emission were examined to determine if they were likely to emit UV radiation: Larger U-B values indicated that the star emitted very little UV radiation, and would not contaminated the UV measurements. These 33 SNRs were analyzed in CCDLAB to determine whether or a measurement of the diffuse emission could be done. 13 of these were isolated enough from nearby UV sources to analyze using box measurements. 5 sources had clear indications of diffuse emission, but the region had too many overlapping stars (i.e. was confused) for a reliable flux measurement to be taken. The remaining 15 sources were removed from the list as there was either no clear indication of SNR emissions within the SNR radius, or the measured flux was too dim compared to the background to result in a reliable measurement.

The result of the above selection process left 25 UV emitting SNRs consisting of 7 without stellar contamination; 13 with stellar contamination which can be separated from the diffuse emission and 5 more with likely diffuse emission but too confused with stars for measurement. The locations of the 20 SNRs in M31 with clear diffuse UV emission and 5 SNRs with likely diffuse emission are shown in Figure 2. We do not consider further the 5 diffuse but confused sources for which reliable UV fluxes could not be obtained. Thus, the number of SNRs for which we can carry out flux measurements is 20.

Properties of the 20 SNRs with detected diffuse UV emission are shown in Table 1. Table 1 lists each SNR's ID numbers, including their original Lee and Stiele (SPH11) IDs, their J2000 coordinates, the optical diameter and error, the likely progenitor type, and their optical and/or X-ray luminosities.

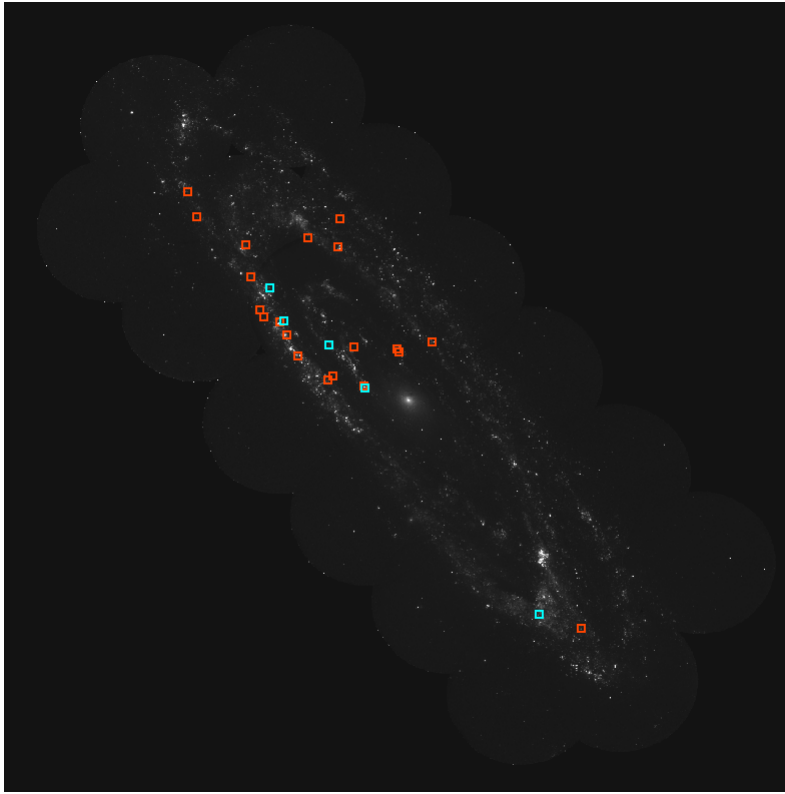


**Figure 2.** Positions of the 20 SNRs with detected diffuse UV emission (red squares) and of the 5 SNRs with likely, but confused, diffuse emission (blue squares), overlaid on the image of M31 in the F148W filter.

**Table 1.** Optical and X-ray data of the 20 UV-emitting SNRs

IDs	Candidates <sup>a</sup>		Coordinates <sup>b</sup>		Observational		SNR		Optical Luminosity <sup>c</sup>		X-ray Luminosity	
	(2)	(3)	R.A.	DEC.	Radii (pc)	Err. <sup>e</sup>	Type	log(H $\alpha$ )	log([SII])	0.35-2keV <sup>e</sup>	0.3-10keV <sup>f</sup>	
SNR	(4)	(5)	(6)	(7)	(8)	(9)	(10)	(11)	(12)	(13)	(14)	
1	5	6	9.9685	40.4951	71		CC	36.88	36.71			
2	45	40	10.5842	41.4652	45.2		CC	36.74	36.52			
3	57	50	10.7236	41.4310	26.8	1.89	Ia	36.49	36.45	3.80E+36		
4	59	52	10.7326	41.4402	59.8		Ia	36.22	36.17			
5	75	67	10.8721	41.3178	46		CC	36.28	36.16			
6	78	70	10.9133	41.4483	25.2	2.12	Ia	36.6	36.56	3.10E+36	1.80E+36	
7	90	78	10.9777	41.8817	37.8		Ia	36.41	36.42			
8	91	79	10.9838	41.7853	90.6		CC	36.49	36.37			
9	94	82	11.0045	41.3515	13		CC	35.47	35.21			
10	98	85	11.0231	41.3364	54.6		CC	36.17	36.02			
11	107	93	11.1101	41.8165	61.6		CC	35.89	36.02			
12	113	98	11.1526	41.4182	69.4		CC	36.97	36.76			
13	121	106	11.1962	41.4891	42	4.83	CC	36.59	36.54	4.40E+35	1.60E+35	
14	128	113	11.2269	41.5312	43		CC	36.06	35.97			
15	136	125	11.2941	41.5476		4.69				3.60E+35		
16	142	125	11.3135	41.5735	69.6		Ia	35.85	35.9			
17	147	130	11.3517	41.6839	44		CC	35.98	35.65			
18	154	137	11.3734	41.7918	66.2		Ia	35.96	36.1			
19	166	147	11.5838	41.8833	89.4		CC	36.49	36.13			
20	169	148	11.6234	41.9695	49.6		CC	36.21	36.13			

NOTE— a) ID number from our initial list of 177 SNRs. b) From Lee & Lee (2014), except for SNR 15, which is from Stiele et al. (2011). c) From Lee & Lee (2014). d) From Stiele et al. (2011). e) From Sasaki et al. (2012). f) From Sasaki et al. (2018).

**Table 2.** M31 SNRs with UV emission

SNR	Coordinates (J2000)		UV Luminosity ( $10^{35}$ erg/s)				
	R.A.	DEC.	F148W	F169M	F172M	N219M	N279N
ID	(hh mm ss)	(dd mm ss)					
1	00 39 52.0	40 29 44.7	50.0±5.1	21.8±2.2			
2	00 42 20.0	41 27 54.7	49.3±4.9	23.9±2.4	9.4±1.0	10.4±1.1	4.2±0.5
3	00 42 53.6	41 25 51.5	46.9±4.7	24.7±2.5	11.4±1.2	14.9±1.5	3.7±0.4
4	00 42 55.4	41 26 22.8	8.1±0.9	4.8±0.6	2.6±0.3	1.7±0.4	0.7±0.2
5	00 43 29.2	41 19 02.0	11.0±1.7	3.9±0.7	1.5±0.3	1.3±0.5	0.3±0.2
6	00 43 39.1	41 26 53.6	43.9±4.4	24.6±2.5	10.6±1.1	13.1±1.4	4.0±0.4
7	00 43 54.2	41 52 54.7	17.1±1.8		3.5±0.4	2.1±0.3	
8	00 43 56.4	41 47 10.1	40.4±4.2		7.0±0.8	5.6±0.6	2.1±0.3
9	00 44 01.0	41 21 05.3	6.2±0.8	3.6±0.5	0.4±0.2	3.6±0.7	0.4±0.2
10	00 44 05.1	41 20 12.7	9.9±1.4		3.7±0.4		0.9±0.2
11	00 44 26.8	41 48 57.4	14.2±2.4		3.4±0.5		
12	00 44 36.4	41 24 57.8	86.3±8.7		17.9±1.8	21.7±2.2	9.0±0.9
13	00 44 46.7	41 29 23.9	38.4±3.9		8.8±0.9	12.6±1.3	4.3±0.4
14	00 44 54.6	41 31 52.2	76.2±8.1		20.9±2.2	20.3±2.1	5.3±0.7
15	00 45 10.7	41 32 53.4	22.9±2.5		4.0±0.5	3.8±0.6	3.6±0.4
16	00 45 15.3	41 34 27.8	14.0±1.7		1.7±0.4	3.6±0.5	3.5±0.4
17	00 45 24.7	41 41 00.3	22.0±2.8		5.0±0.6	6.4±0.7	1.7±0.2
18	00 45 30.0	41 47 36.7	20.3±3.2		3.5±0.5		
19	00 46 20.2	41 53 04.6	28.4±2.9		6.9±0.7		
20	00 46 30.0	41 58 09.4	27.9±2.9		5.6±0.6		

### 3.3. Measurement of SNR UV Luminosities

From the measured fluxes and the known distance to M31, we determine the SNR UV luminosities in the different filters. CCDLAB provides source fitting methods for photometric measurements (Postma & Leahy 2017). The methods include Gaussian and Moffat functional fits, a Curve-of-Growth fit (COG), and a box fit. For diffuse emission Gaussian and Moffat functions, designed for fitting point sources, are not suitable. The COG fit works well to measure all counts within a given radius if there is a good background outside that radius, but does not work well for our diffuse sources usually surrounded by stellar sources. Thus, we use the box method to calculate the fluxes of diffuse emission and to subtract background emission while avoiding stellar emission in both source and background boxes.

The box method yields the total photon counts in a chosen box, which can be square or rectangular. The SNR source counts were measured using different box sizes, generally 4 different sizes from 17 by 17 pixels to 23 by 23 pixels. However, more crowded sources would be measured 2 or 3 times using smaller boxes, and some sources required larger boxes due to their unusual shape. A few sources were large and irregularly shaped. These required a larger box to encapsulate the UV emission, and for these cases small boxes would be used to remove the counts from any stars that fell within the larger box. In order to account for background variations, 6 different measurements were done for each filter using manually chosen boxes. The average of the 6 measurements was used as the background, and the standard deviation of the 6 measurements used as the uncertainty.

The counts for each filter band image were divided by the net exposure time of each image to obtain a count rate. This was corrected for the extended wings of the point-spread-function as given in Table 5 of Tandon et al. (2017). Then the count rate was converted to flux in units of  $\text{erg s}^{-1} \text{cm}^{-2} \text{\AA}^{-1}$  using the flux conversions given in Table 4 of Tandon et al. (2017). Additional uncertainties include Poisson photon counting errors, uncalibrated spatial variations in detector sensitivity, and uncertainties in correction for the wings of the point spread function. These were included in quadrature in the calculation of flux errors. The fluxes and uncertainties were converted into luminosities using the

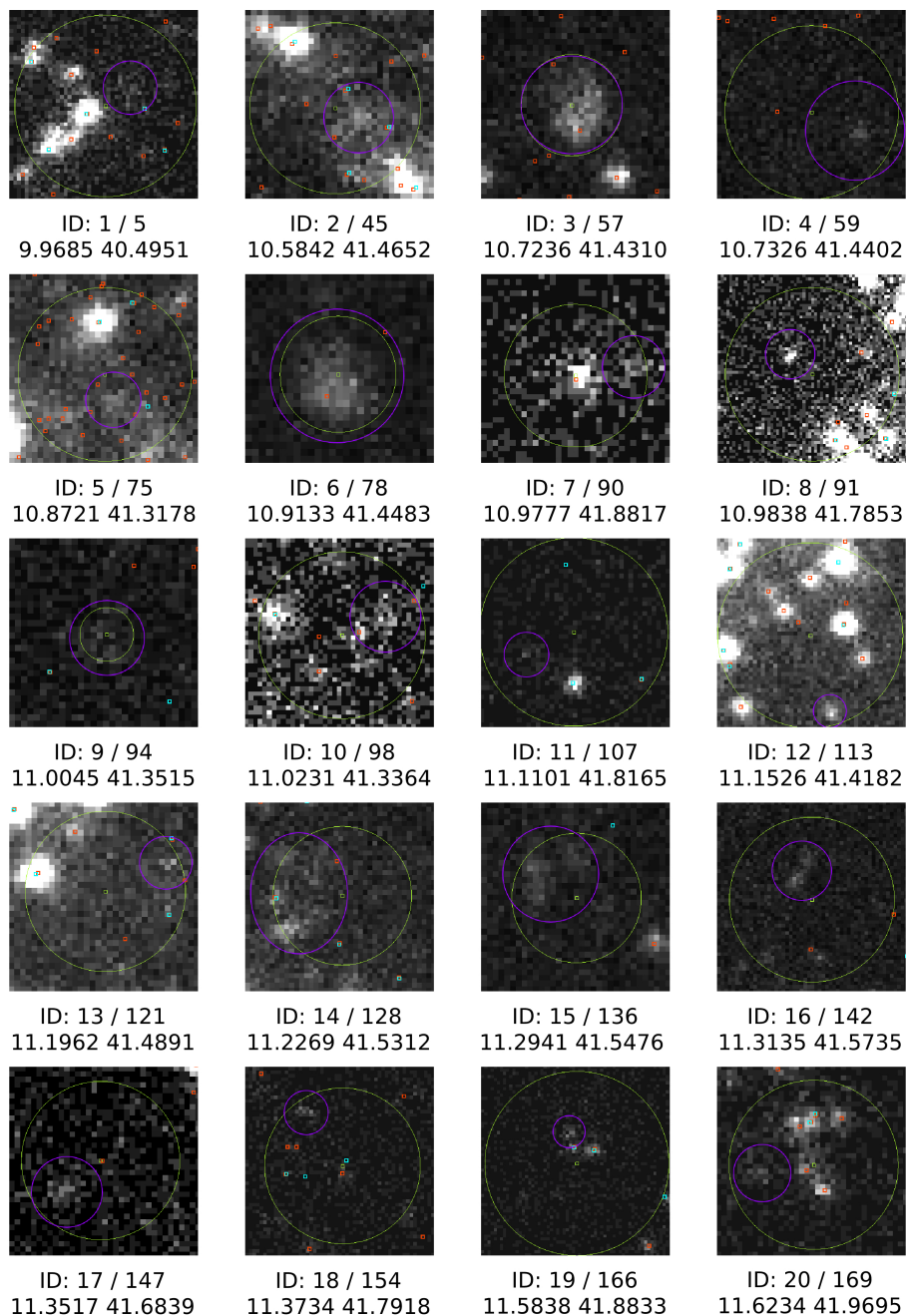


**Figure 3.** The 20 SNRs with UV emission. SNR ID, Candidate ID and J2000 coordinates are given below each panel. The SNR radius is shown by the green circle. The red squares indicate star positions from [Massey et al. \(2016\)](#) and [Massey et al. \(2021\)](#), light blue squares indicate positions of stars from GAIA DR3. The purple circles indicate approximately the areas analyzed to obtain source fluxes.



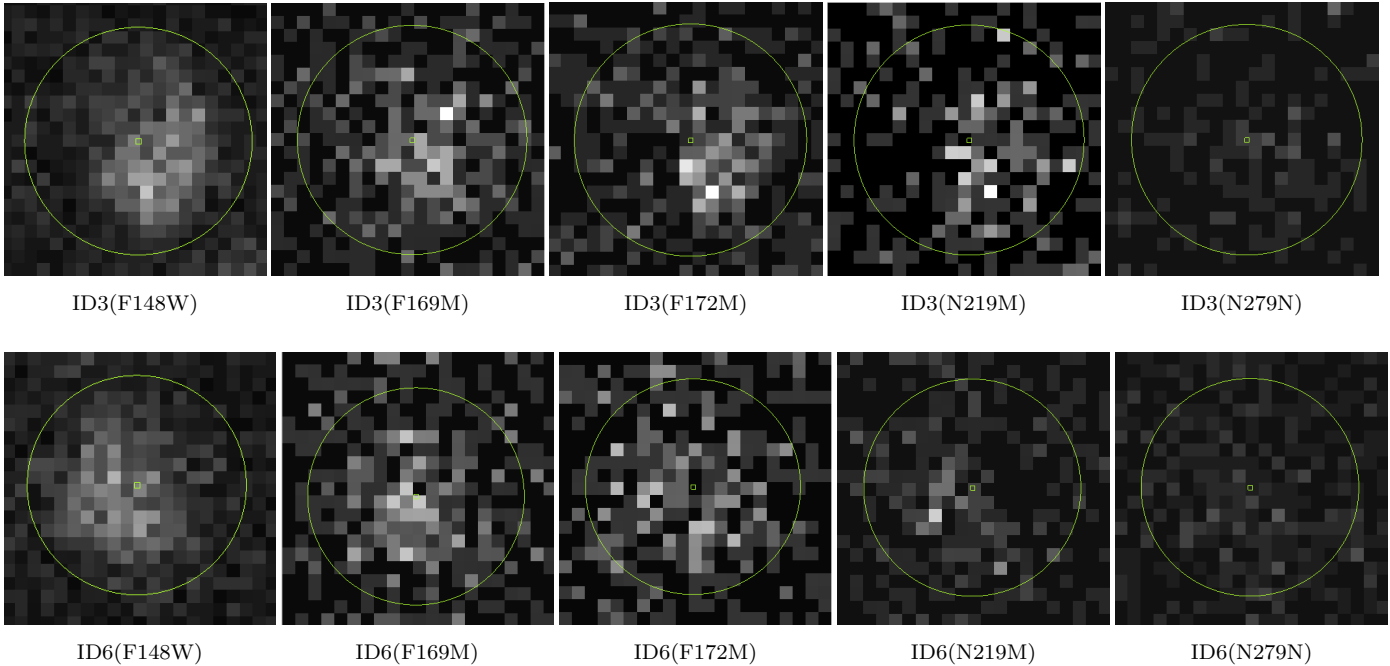


**Figure 4.** Images of two of the best selected SNRs in all 5 filters (F148W, F169M, F172M, N219M and N279N, left to right): top row- ID 3; bottom row- ID 6. The green circles indicates the SNRs radii.

distance to M31 and the effective bandwidth of each filter. The filter effective wavelengths and effective bandwidths are given in Table 3 of [Tandon et al. \(2017\)](#).

## 4. RESULTS AND DISCUSSION

### 4.1. UV emission from M31 SNRs and Catalog of UV emitting SNRs in M31

The images of the 20 M31 SNRs in the F148W band are shown in Figure 3. These sources exhibit diffuse emission which is not associated with stars, although the strength of the diffuse emission varies. Images of two of these sources (ID 3 and ID 6) in all five UVIT filter bands are shown in Figure 4. The catalog of 20 SNRs in M31 with luminosities in the detected UVIT bands is given in Table 2. Because of some overlap of the fields, some SNRs were imaged in two different fields in the same filter. The reported band luminosity and uncertainty for those are the average of these measurements.

The spectral shape of each source is shown in Figure 5, panels (a) and (b). The F148W filter luminosity is the largest for all SNRs analyzed, in part caused by the wider effective bandwidth for the F148W filter. The other filter band luminosities vary in prominence, however the spectral shapes of the 20 M31 SNRs are similar.

### 4.2. Comparison of UV-emitting M31 SNRs with known UV-emitting SNRs

The spectra of known UV-emitting SNRs shows that their emission in the UVIT filter bands would be dominated by emission lines, with a small contribution from continuum radiation. A list of UV emission lines measured in known SNRs ([Fesen & Hurford 1996](#)) is presented in Table 3, together with the UVIT filter bands that contain these lines. These SNRs include 3 Galactic SNRs- the Cygnus Loop ([Raymond et al. 1980, 1981, 1988](#)), Vela ([Raymond et al. 1981](#)), and Puppis A ([Blair et al. 1995](#)); 3 SNRs in the Large Magellanic Cloud- N132D ([Blair et al. 2000](#)), N49 ([Vancura et al. 1992](#)), and N103B ([Blair et al. 2020](#)); and 1 SNR in the Small Magellanic Cloud- E0102-7219 ([Blair et al. 1989, 2000](#)). Table 4 lists these SNRs, with SNR Type, distance, and aperture size for the line flux measurements given in the references.

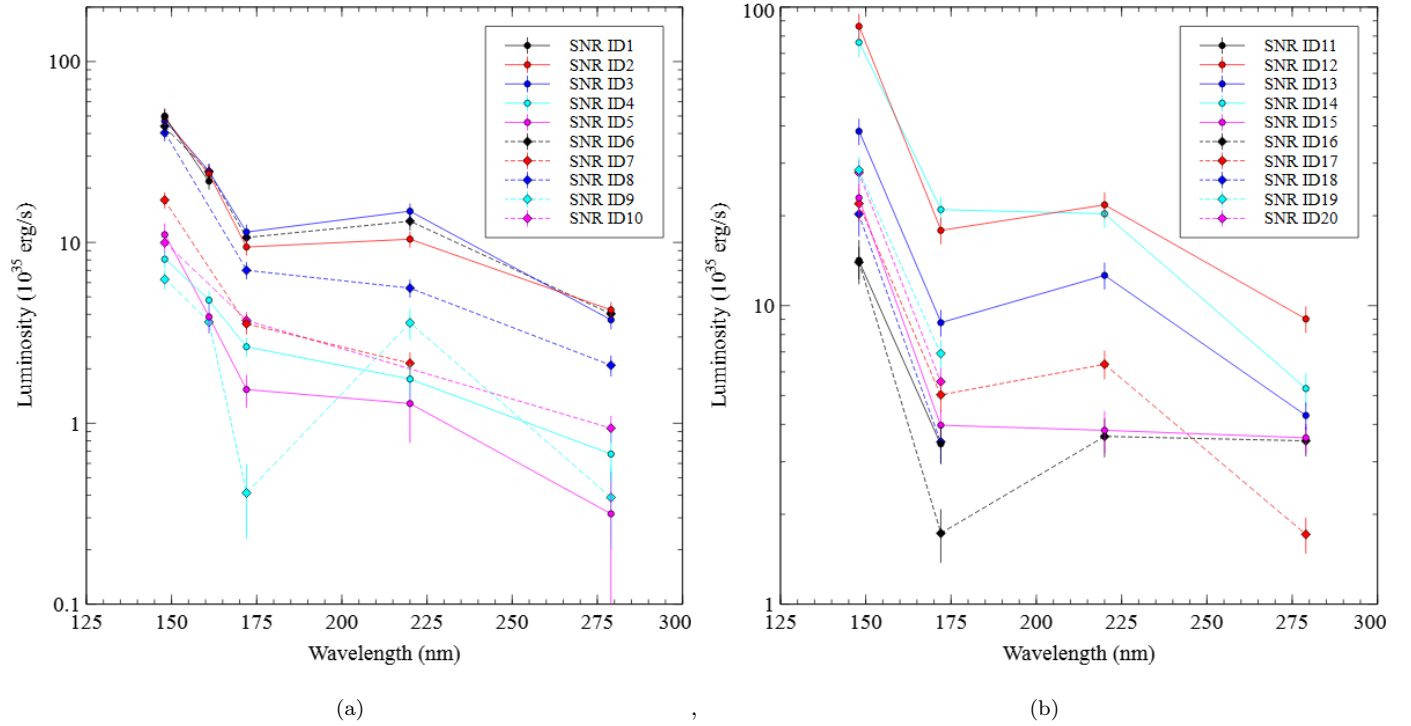


Figure 5. Spectrophotometry of the 20 SNRs: (a) SNR ID's 1 to 10; (b)SNR ID's 11 to 20.

Table 3. Ultraviolet emission lines known SNRs (from Fesen & Hurford 1996) and the UVIT filter bands which contain those lines.

$\lambda$ (Å)	Ion	F148W	F169M	F172M	N219M	N279N
1334.53	C II	X				
1355.6	O I	X				
1371.29	O V	X				
1393.76	Si IV	X				
1397.20, 1399.77	O IV]	X				
1398.13, 1404.77	S IV]	X				
1402.77	Si IV	X				
1483.32, 1486.50	[N IV],N IV]	X	X			
1533.43	Si II	X	X			
1548.20, 1550.77	C IV	X	X			
1574.8	[Ne V]	X	X			
1601, 1602	[Ne IV]	X	X			
1640 blend	He II	X	X	X		
1660.81, 1666.15	O III]	X	X	X		
1670.81	Al II	X	X	X		
1730 blend	N III]	X	X	X		
1746.82, 1748.61	N III]	X	X	X		
2320.95, 2331.40	[O III]				X	
2323.50, 2324.69	C II]				X	
2328.51, 2334.40	Si II]				X	
2795.52, 2802.70	Mg II					X

**Table 4.** Known UV-emitting SNRs and estimated UVIT filter band luminosities calculated from measured line fluxes

SNR	Type	Location	Distance (pc)	Estimated UVIT Filter Band Luminosity (erg/s)					Aperture Size	Source
				F148W	F169M	F172M	N219M	N279N		
Cygnus Loop	CC	Milky Way	725	5.82E+36	4.48E+36	2.29E+36	1.53E+36	-	10" x 20"	a
				3.62E+36	2.77E+36	8.46E+35	1.17E+36	2.10E+35	4 x 10" x 20"	b
Vela	CC	Milky Way	250	5.18E+36	4.12E+36	2.28E+36	1.39E+36	-	3 x 3.8" x 12.4"	c
PuppisA	CC	Milky Way	2,146	3.56E+35	2.53E+35	8.24E+34	6.07E+34	-	4 x 10" x 20"	b
N49	CC	LMC	2,146	1.86E+33	1.43E+33	2.88E+32	-	-	10" x 56"	d
N103B	Ia	LMC	50,000	5.47E+37	4.94E+37	8.40E+36	2.60E+37	1.30E+37	5 x 10" x 20"	e
N132D	CC	LMC	45,990	4.62E+35	3.19E+35	5.06E+34	-	-	2.5" (circular)	f
N132D	CC	LMC	52,000	4.34E+34	2.51E+34	8.07E+33	6.21E+33	8.49E+33	3 x 1" (circular)	g
E0102-7219	CC	SMC	64,386	6.28E+33	3.45E+33	1.09E+33	5.28E+32	9.24E+32	1" x 1"	g
				4.05E+35	2.12E+35	3.18E+34	1.50E+34	1.92E+34	10" x 20"	h

NOTE—a) Raymond et al. (1980). b) Raymond et al. (1981). c) Raymond et al. (1988). d) Blair et al. (1995). e) Vancura et al. (1992). f) Blair et al. (2020). g) Blair et al. (2000). h) Blair et al. (1989).

We estimated the UVIT band luminosities for the known SNRs by summing the published luminosities or fluxes (converted to luminosities) of the detected emission lines which fall within each UVIT filter, as listed in Table 3. The results of this are given in columns 5 through 9 of Table 4 and the band luminosities vs. the effective wavelengths of the UVIT filter bands are shown in panel (a) of Figure 6. Although the band luminosities of the different sources are quite variable, the F148W luminosity is the brightest. That band includes more emission lines than the other bands (see Table 3).

Supernovae and SNRs can be categorized into two separate types: thermonuclear runaway (Type Ia) and core collapse (CC). The small sample of known SNRs with UV spectroscopy includes only one type Ia SNR (N103B). This SNR has band luminosities (panel (a) of Figure 6) which does not appear different to the CC-type SNRs. Scaled band luminosities are defined as the band luminosities for each SNR divided by the F148W band luminosity for that SNR. The scale band luminosities of the seven known UV-emitting SNRs are shown in panel (b) of Figure 6. They are all quite similar, with factor  $\sim 2$  variations between the different SNRs.

Although UV spectroscopic data for the M31 SNRs does not exist, we can compare the UV emission of the M31 sources to known UV-emitting SNRs by comparing the UVIT band luminosities. For several of the known SNRs, the aperture only covered part of the area of the SNR, so that we do not have a good measurement of the line luminosities over the whole SNR. The extrapolation from the aperture to the whole SNR is a highly uncertain factor because of line brightness variations over the face of the SNR. However, if the line ratios are nearly constant over the face of the SNR, the scale band luminosities should be representative of the spectral shapes of the whole SNR. Thus we compare the spectral shapes of the known SNRs to one another and to the M31 SNRs using the scaled band luminosities.

For the band luminosities, known SNRs (panel (a) of Figure 6) show larger variations than the 20 new UV emitting SNRs in M31 (panels (a) and (b) of Figure 5). This is, in part, caused by the different fractions of the SNR area measured in the aperture of the spectroscopic observations (Table 3). However, the scaled band luminosities (panels (b) of Figure 6) show that the spectral shapes of the known SNRs are quite similar. The F148W value is the largest, followed by the F169M value, then with similar values in the remaining 3 bands (F172M, N219M and N279N). The scaled band luminosities of the 20 M31 SNRs (panels (c) and (d) of Figure 6) have remarkably similar variations to the known SNRs. The strong similarity of the rescaled band luminosities of the newly detected 20 M31 SNRs to known UV-emitting SNRs (Figure 6) is evidence that the detected UV emission is from the SNR, rather than from foreground or background objects.

This current list of 20 UV-emitting SNRs in M31 is likely incomplete. The interstellar extinction of UV light from M31 by the Milky Way's ISM is small, but the ISM of M31 can have significant extinction. The extinction has been measured for stellar clusters in M31 using UVIT photometry of stellar clusters (Leahy et al. 2022b): the mean extinction is  $E(B - V) = 0.24$  and ranges from 0 to 0.6. Thus SNRs within or on the farside of M31's disc may be undetected because of extinction. More than half (Section 3.2) of the SNRs from the original list of 177 were excluded

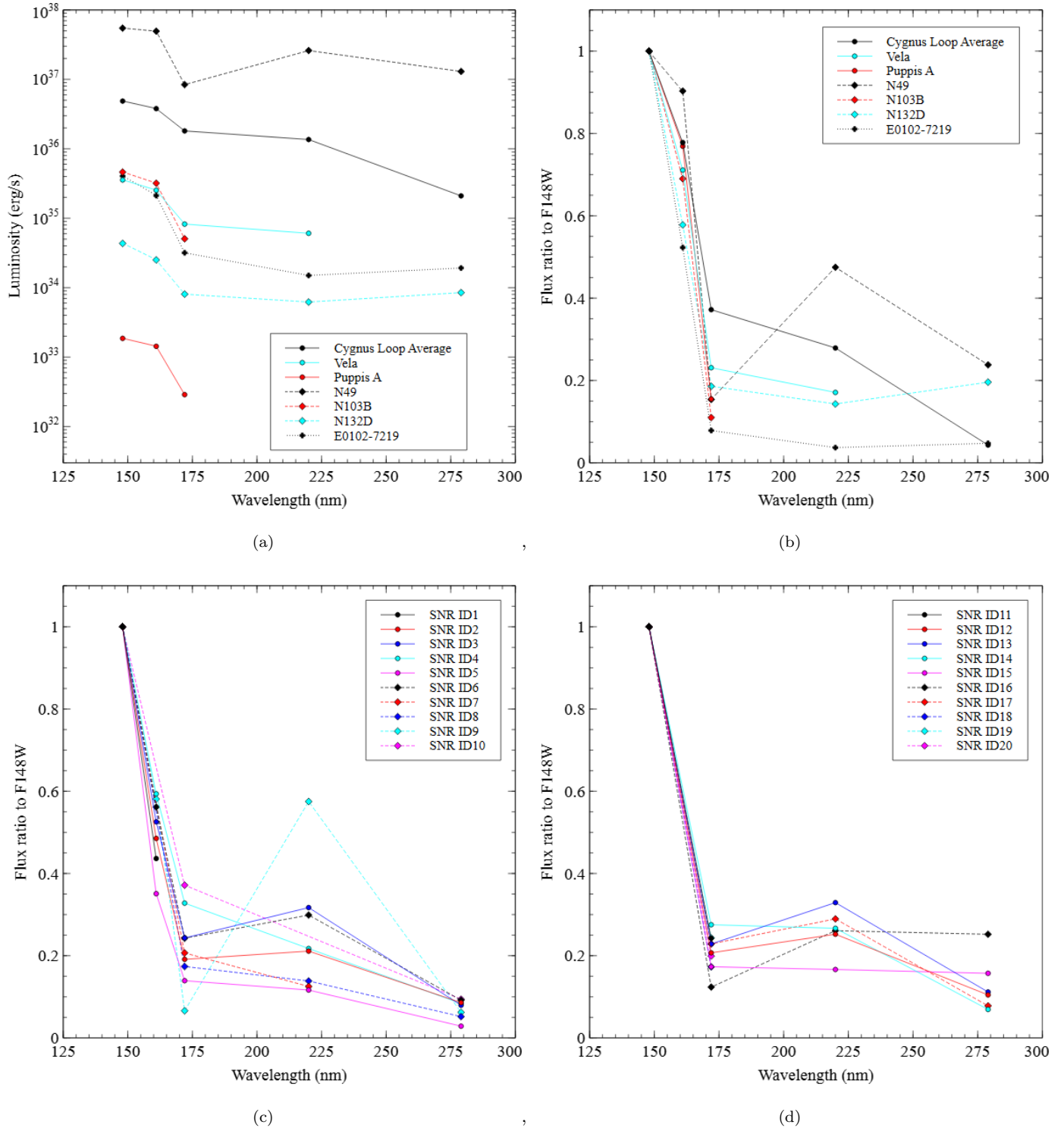


**Figure 6.** Spectral shape of 7 known UV-Emitting SNRs: (a) estimated band luminosities (for Cygnus Loop the average of the 3 values and for E0102-7219 the second listed values from Table 4 are plotted); (b) scaled band luminosities (luminosity divided by the F148W luminosity of each SNR). Scaled band luminosities for the SNRs in M31: (c) SNR ID's 1 to 10; (d) SNR ID's 11 to 20.

**Table 5.** Models for 6 M31 SNRs with X-ray spectra

SNR <sup>(a)</sup>	Type <sup>(b)</sup>	$M_{ej}^{(c)}$	(s,n) <sup>(d)</sup>	Shock <sup>(e)</sup>	Age	E0	density	$\dot{M}/(4\pi V_w)$	$kT_2^{(e)}$	$EM_2^{(e)}$	Consistent? <sup>(f)</sup>
SPH11 ID		$M_\odot$			(yr)	( $10^{51}$ erg)	( $\text{cm}^{-3}$ )	(gm/cm)	(keV)	( $10^{58}\text{cm}^{-3}$ )	
1066(UV)	Ia	1.2	(0,7)	fwd	1970	12.1	0.33		20.5	$5.76 \times 10^{-3}$	Y
1066(UV)	Ia	1.2	(2,12)	fwd	324	33.2		$9.39 \times 10^{13}$	0.70	48.4	N
1066(UV)	Ia	1.2	(2,12)	rev	133	16.0		$3.66 \times 10^{13}$	20.6	1.12	Y
1275(UV)	Ia	1.2	(0,7)	fwd	14040	0.311	0.594		1.243	$8.23 \times 10^{-3}$	Y
1275(UV)	Ia	1.2	(2,12)	fwd	2950	0.387		$1.50 \times 10^{14}$	0.035	131	N
1275(UV)	Ia	1.2	(2,12)	rev	636	6.76		$5.85 \times 10^{13}$	1.03	3.05	Y
1055	(unk.)	5	(0,7)	fwd	7220	0.234	0.080		0.131	0.421	Y
1055	(unk.)	5	(2,12)	fwd	1420	0.769		$8.65 \times 10^{13}$	0.035	96.6	N
1055	(unk.)	5	(2,12)	rev	292	14.8		$3.37 \times 10^{13}$	1.03	2.24	Y
1234	CC	10	(0,7)	fwd	23300	1.02	0.488		0.683	$9.33 \times 10^{-2}$	Y
1234	CC	10	(2,12)	fwd	5400	2.03		$3.18 \times 10^{14}$	0.033	368	N
1234	CC	10	(2,12)	rev	1030	38.8		$6.35 \times 10^{13}$	0.974	2.24	Y
1535	CC	10	(0,7)	fwd	18500	0.344	0.320		0.254	$8.19 \times 10^{-2}$	Y
1535	CC	10	(2,12)	fwd	3360	2.49		$1.30 \times 10^{14}$	0.035	78.8	N
1535	CC	10	(2,12)	rev	782	37.3		$5.07 \times 10^{13}$	1.03	1.83	Y
1599	CC	10	(0,7)	fwd	18200	1.143	0.568		0.774	1.120	Y
1599	CC	10	(2,12)	fwd	3640	3.45		$2.98 \times 10^{14}$	0.044	361	N
1599	CC	10	(2,12)	rev	807	56.9		$1.16 \times 10^{14}$	1.299	8.37	Y

NOTE—(a) The UV-emitting SNRs are marked with (UV). (b) Type Ia (Ia), core collapse (CC) or unknown (unk.). (c) Ejecta mass taken as  $1.2M_\odot$  for Ia,  $10M_\odot$  for CC or  $5M_\odot$  for unk. (d) s=power law index for circumstellar medium density: constant s=0, or wind s=2; n=power law index for ejecta density. (e) Measured  $kT$  and  $EM$  are assumed to be from forward shock (fwd) or from reverse shock (rev); if "fwd" then  $kT_2$  and  $EM_2$  are the predicted values for the reverse shock; if "rev" then  $kT_2$  and  $EM_2$  are the predicted values for the forward shock. (f) Is the predicted  $EM_2$  small enough to be consistent with observations? (Y=yes), (N=no).

because of confusion with stellar emission: there was not enough diffuse emission separated from overlapping stars within the SNR radius for detection.

#### 4.3. Physical conditions of the 6 M31 SNRs with X-ray spectra

To determine density of environment and evolution status of SNRs, X-ray observations of the thermally emitting shocked gas are required. There are 6 SNRs in M31 which have had their X-ray spectra analyzed with hot plasma models from shocked gas, from Sasaki et al. (2012) and Sasaki et al. (2018). We use the spectral parameters for SPH11 SNRs 1050 and 1066 from Sasaki et al. (2012) and for SPH11 SNRs 1234, 1275, 1535 and 1599 from Sasaki et al. (2018)<sup>2</sup>. The emission measures ( $EM$ ) for each SNR was calculated from "norm" or from the flux, if no "norm", using XSPEC and the best fit spectral model.

The modelling software used is SNRpy (Leahy et al. 2019; Leahy & Williams 2017) which is based on the unified models of SNR evolution of Truelove & McKee (1999), with extensions added, including non-equilibrium ionization. For each SNR, we fit the measured shocked-gas temperature  $kT$  and emission measure  $EM$  for 3 different cases: i) explosion in a uniform environment (s=0) and emission from the forward-shocked gas; ii) explosion in a stellar wind (s=2) and emission from the forward-shocked gas; and iii) explosion in a stellar wind (s=2) and emission from the reverse-shocked gas. Explosions in a uniform medium lead to much brighter emission from forward-shocked gas, but explosions in a wind environment can lead to either brighter emission from the forward-shocked gas or from the reverse-shocked gas. The results of the models are given in Table 5. Because the measured X-ray spectrum is for the brighter component (i.e. forward or reverse-shocked), we mark the models which are consistent with the observations (i.e. measured  $EM$  larger than  $EM_2$ ) in the Table. Emission from the forward-shock gas in a uniform medium (s=0) or emission from the reverse-shocked gas in a stellar wind (s=2) are consistent with observations. Other information can help to select a preferred model for each SNR. E.g., SNRs with energy above  $10^{52}$  erg should be rare (Leahy &

<sup>2</sup> SPH11 1234 was analyzed in both: we used the newer analysis from the later reference.

Filipović 2022c; Leahy et al. 2020b; Leahy 2017). This disfavors the  $(s,n)=(2,12)$  reverse-shock models for SPH11 1234, 1535 and 1599. The energies, ages and densities (or stellar wind parameters) are reasonable for the other models.

The 2 UV-emitting SNRs with X-ray spectra, SPH11 1066 and 1275, are marked with (UV) in Table 5. The clear difference between the UV emitting SNRs and the UV non-detected SNRs is that the 2 UV-emitting SNRs are Type Ia. Because of the large age of Type Ia progenitors compared to CC progenitors, Type Ia are expected to be at significant height above the disk plane, and thus to have low extinction. The models for the 6 SNRs have a range of ages, explosion energies and densities, and the sample is too small to see systematic differences in the ages, densities or explosion energies between the UV-detected and non-detected SNRs. One would expect the column density (given in Sasaki et al. 2012 and Sasaki et al. 2018) to be smaller for the UV-detected SNRs. The column densities are small, with large uncertainties, except for SPH11 1599 which is not detected in UV. Better determination of column densities with better X-ray spectra are needed to confirm the relation between UV-detection and low column density.

#### 4.4. Comparison of numbers of M31 SNRs in different wavebands

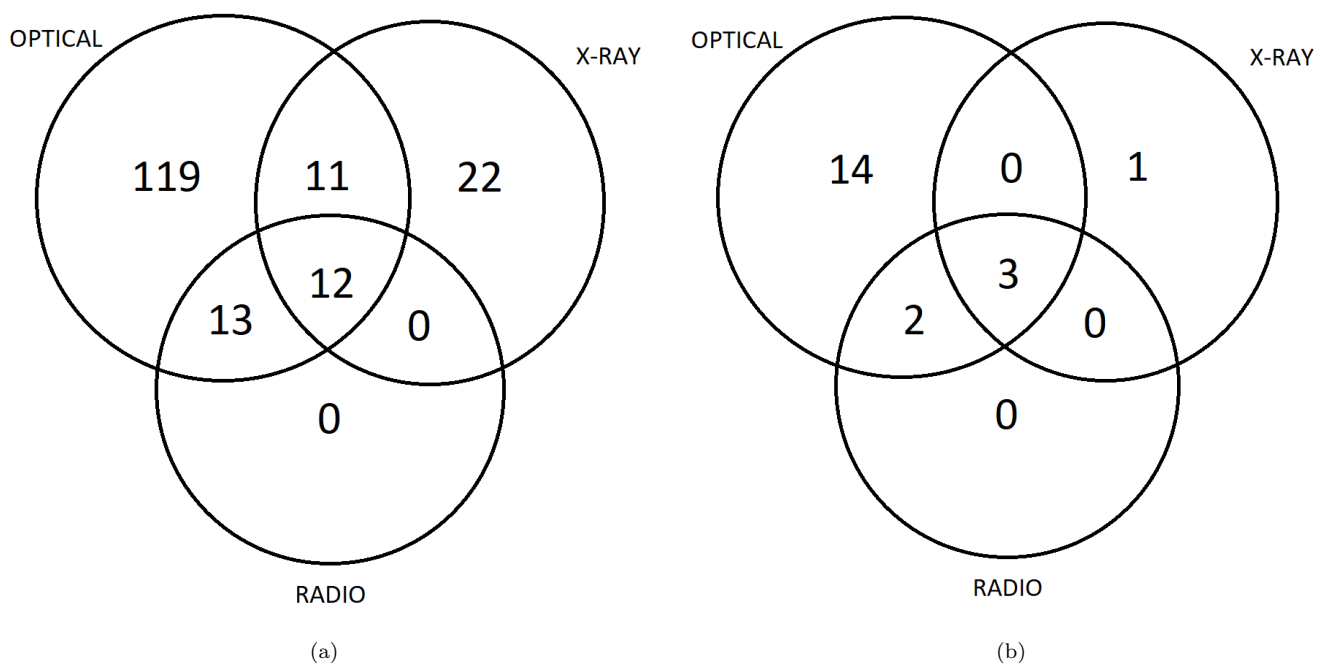


**Figure 7.** Venn diagrams for SNRs in M31 detected in different wavebands (optical, X-ray and radio: (a): all SNRs; (b): for the 20 SNRs detected in UV (this work).

The 177 SNRs in M31 were detected in different wavebands; optical, X-ray and radio, prior to the current work. Panel (a) of Figure 7 shows the numbers of SNRs detected in single and multiple wavebands using a Venn diagram. Pannuti et al. (2000) shows similar Venn diagrams (optical, radio, and x-ray detected SNRs) for the nearby galaxies M33 and NGC300. M33 has a total number of 109 SNRs and SNR candidates and NGC300 has a total of 44, compared to the total of 177 SNRs and SNR candidates for M31. For all 3 galaxies (M31, M33 and NGC300), optically-detected SNRs dominate with fractions of detected SNRs of 155/177, 79/109 and 28/44, respectively. The X-ray and radio detections are significantly smaller fractions: the X-ray detected fractions are 45/177, 21/109, and 6/44 respectively; and the radio detected fractions are 25/177, 53/109 and 17/44, respectively. The optically detected fractions are similar ( $\sim 0.6 - 0.9$ ) for all 3 galaxies; the radio detected fractions higher for M33 and NGC300 ( $\sim 0.4 - 0.5$ ) than for M31 ( $\sim 0.15$ ), and the X-ray detected fraction higher for M31 ( $\sim 0.25$ ) than for M33 and NGC300 ( $\sim 0.15 - 0.2$ ). This is probably the result of the intensive X-ray observations of M31 (Sasaki et al. 2012, 2018) compared to the other two galaxies. The three sets of optically-detected, radio-detected and X-ray detected SNRs show little overlap for all three galaxies. This is consistent with the opposing selection effects for these 3 wavebands, as discussed in Pannuti

*et al.* (2000): SNRs identified through optical represent those located in regions with relatively low confusion from H $\alpha$  emission, well away from star-forming regions; radio-selected SNRs are biased toward star-forming regions; and X-ray SNRs are selected for soft X-ray spectra and association with H II regions, so are biased against SNRs with hard spectra and no optical counterparts.

Bozzetto *et al.* (2017) considers the statistics of optical, radio and X-ray detections for the Large Magellanic Cloud (LMC). The Venn diagram of SNRs for the LMC shows most SNRs (47 of 59) are detected in all three bands. This is probably a result of sensitivity to luminosity because of the closer distance of the LMC ( $\sim 20$  times closer than the other nearby galaxies discussed above). The Venn diagrams given in Bozzetto *et al.* (2017) include NGC300 and M33, with similar numbers to those given in Pannuti *et al.* (2000), and M31 with results similar to Figure 7 here. The other galaxies with Venn diagrams in Bozzetto *et al.* (2017) are the Small Magellanic Cloud (SMC), NGC7793, NGC 6946, NGC 55, and one diagram for NGCs 2403, 3077, 4214, 4395, 4449 and 5204 combined (hereafter referred to as "NGCcombined"). For the SMC, which is also nearby, the diagram is similar to that for the LMC with most SNRs detected in all 3 bands. The diagrams for NGCcombined, NGC 7793 and NGC 6946 are dominated by SNRs detected in optical only, like M31, M33 and NGC 300. NGC 55 has too few SNRs (6 total) to draw conclusions on numbers. The differences are likely the result of the differing sensitivities of the observations in the different wavebands for each of the galaxies, as discussed by Bozzetto *et al.* (2017).

The 20 UV-emitting SNRs in M31 are listed in Table 1. The other wavebands in which these 20 SNRs are detected are as follows. Sources 1, 2, 4, 5, 8, 10, 11, 12, 14, 16, 17, 18, 19, and 20 were listed only in Lee & Lee (2014) (optical); sources 7 and 9 were listed in Lee & Lee (2014) and in Braun & Walterbos (1993)(optical & radio); source 15 was listed only in Sasaki *et al.* (2012) (X-ray) and sources 3, 6, and 13 were listed in all 3 (optical, X-ray, & radio). Panel (b) of Figure 7 shows the numbers of UV-emitting SNRs detected in optical, X-ray and radio. Nearly all of the UV-emitting SNRs (19 of 20) are detected in optical. This is not surprising because the emission mechanisms for UV and optical are most similar: forbidden and recombination lines from shock-ionized gas. In contrast, the radio emission mechanism is synchrotron from shock-accelerated electrons and the the emission mechanism is primarily thermal bremsstrahlung with some contribution from lines.

The total number of UV-emitting SNRs in M31 is similar to the number radio emitting SNRs (20 vs. 25) but much smaller than numbers of optical or X-ray emitting SNRs. The fractions of UV-emitting SNRs in M31 are: 19/155 (optical), 5/25 (radio) and 4/45 (X-ray). These have not been measured for other galaxies yet, but are similar ( $\sim 0.1 - 0.2$ ) for the 3 different categories. This indicates that the UV-selection criterion is different than the optical, radio and X-ray criteria listed above. The most important expected UV detection criterion is source extinction. This is important for the 7 previously known SNRs, which all have low extinction (see references in Table 4). The UV extinction to SNRs in M31 is dominated by line-of-sight distance through M31's disk<sup>3</sup>. For M31 SNRs detected in optical, radio and X-ray, the disk extinction is small at those wavelengths so they should be detected independent of distance into the disk. The SNRs detected in UV will be those on the near side of the disk. The fraction detected in UV to other wavebands should be determined by extinction, i.e. disk geometry, and thus approximately constant and equal to the fraction of disk which is on the near side of M31 and with low extinction in UV. The visible to UV extinction curve (Fitzpatrick & Massa 2007) has  $E(\lambda-V)/E(B-V) \sim 3.5$  to 7 (average  $\sim 5$ ) for  $\lambda = 120$  nm to 280 nm (with the peak at 220 nm). Typical measured  $E(B-V)$  values in M31 are in the range 0.0 to 0.6 (Leahy *et al.* 2022b), which yields  $E(\lambda-V)$  from 0 to 3 mag, and extinction factors from 1 to 0.06. The fraction of UV to optical SNRs in M31 (19/155= 0.12, Figure 7) is consistent with that expected from extinction, but the differing sensitivity of UV and optical observations could also affect the fraction.

## 5. CONCLUSION

Using the survey images of M31 carried out by Astrosat's UVIT, we searched for diffuse UV-emission from M31 SNRs. SNRs for analysis were obtained from previous optical, X-ray and radio surveys for SNRs in M31. We used stellar catalogues and the UV images to remove SNRs contaminated with stellar emission, enabling us to detect 20 SNRs with diffuse UV emission in M31. Band fluxes for the five observed UVIT filters, F148W, F169M, F172M, N219M and N279N, were measured for these 20 SNRs to obtain band luminosities. The result is the first catalog of UV emitting SNRs in M31.

<sup>3</sup> The Milky Way contribution to extinction is small in the direction of M31

The band luminosities of the UV-emitting SNRs were compared to the band luminosities computed from the spectra for seven previously known UV-emitting SNRs in the Milky Way, the LMC, and the SMC. We find similar spectral shapes between the known SNRs and the M31 SNRs. The spectral shapes and the diffuse nature of the emission together form good evidence that the UV emission from the 20 M31 SNRs is dominated by line emission, like known SNRs, and that the UV emission is associated with the SNRs.

For the small sample of 6 SNRs in M31 with X-ray spectral models, we apply SNR models to obtain their physical characteristics. The 2 UV-emitting X-ray SNRs are Type Ia, the other 4 X-ray SNRs are CC type. Type Ia indicates positions above the disk plane in M31. The two UV-emitting X-ray SNRs have low measured extinction in X-rays, so that it is consistent that the detection of UV emission is related to low extinction.

We compare the numbers of SNRs detected in M31 for different wavebands (optical, radio and X-ray) to those detected in other nearby galaxies given by Pannuti et al. (2000) and Bozzetto et al. (2017). This confirms the somewhat opposing selection effects for detecting SNRs in the different wavebands, as discussed by Pannuti et al. (2000). 19 of the 20 UV-emitting SNRs are detected in optical, which is expected because the emission mechanisms for both UV and optical are forbidden and recombination lines from shock-ionized gas.

It is desirable to carry out spectroscopic observations to confirm the line nature of the UV emission from these SNRs, although spectroscopy will be difficult for the typically crowded regions in M31 where the SNRs are located.

This work was supported by a grant from the Canadian Space Agency. The authors thank the reviewer for making a number of suggestions to improve this manuscript.

## REFERENCES

- Bailer-Jones, C. A. L., Rybizki, J., Fouesneau, M., et al. 2021, *AJ*, 161, 147. doi:10.3847/1538-3881/abd806
- Benvenuti, P., Dopita, M., & Dodorico, S. 1980, *ApJ*, 238, 601. doi:10.1086/158017
- Blair, W. P., Raymond, J. C., Danziger, J., et al. 1989, *ApJ*, 338, 812. doi:10.1086/167238
- Blair, W. P., Long, K. S., Vancura, O., et al. 1991, *ApJL*, 379, L33. doi:10.1086/186147
- Blair, W. P., Raymond, J. C., Long, K. S., et al. 1995, *ApJL*, 454, L35. doi:10.1086/309757
- Blair, W. P., Morse, J. A., Raymond, J. C., et al. 2000, *ApJ*, 537, 667. doi:10.1086/309077
- Blair, W. P., Ghavamian, P., Raymond, J. C., et al. 2020, *ApJ*, 902, 153. doi:10.3847/1538-4357/abb3c7
- Bozzetto, L. M., Filipović, M. D., Vukotić, B., et al. 2017, *ApJS*, 230, 2. doi:10.3847/1538-4365/aa653c
- Braun, R. & Walterbos, R. A. M. 1993, *A&AS*, 98, 327
- Dong, H., Olsen, K., Lauer, T., et al. 2018, *MNRAS*, 478, 5379. doi:10.1093/mnras/sty1381
- Duric, N. 2000, *Proceedings 232. WE-Heraeus Seminar*, 179
- Fesen, R. A. & Hurford, A. P. 1996, *ApJS*, 106, 563. doi:10.1086/192348
- Fitzpatrick, E. L. & Massa, D. 2007, *ApJ*, 663, 320. doi:10.1086/518158
- Galvin, T. J. & Filipovic, M. D. 2014, *Serbian Astronomical Journal*, 189, 15. doi:10.2298/SAJ140505002G
- Green, D. A. 2019, *Journal of Astrophysics and Astronomy*, 40, 36. doi:10.1007/s12036-019-9601-6
- Kong, A. K. H., Sjouwerman, L. O., Williams, B. F., et al. 2003, *ApJL*, 590, L21. doi:10.1086/376687
- Leahy, D. A. 2017, *ApJ*, 837, 36. doi:10.3847/1538-4357/aa60c1
- Leahy, D. A. & Williams, J. E. 2017, *AJ*, 153, 239. doi:10.3847/1538-3881/aa6af6
- Leahy, D. A., Bianchi, L., & Postma, J. E. 2018, *AJ*, 156, 269. doi:10.3847/1538-3881/aae9e8
- Leahy, D., Wang, Y., Lawton, B., et al. 2019, *AJ*, 158, 149. doi:10.3847/1538-3881/ab3d2c
- Leahy, D. A., Postma, J., Chen, Y., et al. 2020, *ApJS*, 247, 47. doi:10.3847/1538-4365/ab77a9
- Leahy, D. A., Ranasinghe, S., & Gelowitz, M. 2020, *ApJS*, 248, 16. doi:10.3847/1538-4365/ab8bd9
- Leahy, D., Morgan, C., Postma, J., et al. 2021, *International Journal of Astronomy and Astrophysics*, 11, 151. doi:10.4236/ijaa.2021.112009
- Leahy, D., Buick, M., Postma, J., et al. 2021, *AJ*, 161, 215. doi:10.3847/1538-3881/abe9b3
- Leahy, D., Seminoff, N., & Leahy, C. 2022, *AJ*, 163, 138. doi:10.3847/1538-3881/ac4cca
- Leahy, D., Buick, M., & Leahy, C. 2022, *AJ*, 164, 183. doi:10.3847/1538-3881/ac9058
- Leahy, D. A. & Filipović, M. D. 2022, *ApJ*, 931, 20. doi:10.3847/1538-4357/ac6025
- Lee, J. H. & Lee, M. G. 2014, *ApJ*, 786, 130. doi:10.1088/0004-637X/786/2/130



- Maggi, P., Filipović, M. D., Vukotić, B., et al. 2019, *A&A*, 631, A127. doi:10.1051/0004-6361/201936583
- Magnier, E. A., Lewin, W. H. G., van Paradijs, J., et al. 1992, *A&AS*, 96, 379
- Magnier, E. A., Prins, S., van Paradijs, J., et al. 1995, *A&AS*, 114, 215
- Massey, P., Neugent, K. F., & Smart, B. M. 2016, *AJ*, 152, 62. doi:10.3847/0004-6256/152/3/62
- Massey, P., Neugent, K. F., Levesque, E. M., et al. 2021, *AJ*, 161, 79. doi:10.3847/1538-3881/abd01f
- McConnachie, A. W., Irwin, M. J., Ferguson, A. M. N., et al. 2005, *MNRAS*, 356, 979. doi:10.1111/j.1365-2966.2004.08514.x
- Minkowski, R. 1939, *ApJ*, 89, 156. doi:10.1086/144037
- Pannuti, T. G., Duric, N., Lacey, C. K., et al. 2000, *ApJ*, 544, 780. doi:10.1086/317238
- Page, M. J., Brindle, C., Talavera, A., et al. 2012, *MNRAS*, 426, 903. doi:10.1111/j.1365-2966.2012.21706.x
- Postma, J. E. & Leahy, D. 2017, *PASP*, 129, 115002. doi:10.1088/1538-3873/aa8800
- Postma, J. E. & Leahy, D. 2021, *Journal of Astrophysics and Astronomy*, 42, 30. doi:10.1007/s12036-020-09689-w
- Press, W. H., Teukolsky, S. A., Vetterling, W. T., et al. 1992, Cambridge: University Press, —c1992, 2nd ed.
- Raymond, J. C., Hartmann, L., Black, J. H., et al. 1980, *ApJ*, 238, 881. doi:10.1086/158050
- Raymond, J. C., Black, J. H., Dupree, A. K., et al. 1981, *ApJ*, 246, 100. doi:10.1086/158902
- Raymond, J. C., Hester, J. J., Cox, D., et al. 1988, *ApJ*, 324, 869. doi:10.1086/165945
- Raymond, J. C., Blair, W. P., Long, K. S., et al. 1997, *ApJ*, 482, 881. doi:10.1086/304183
- Sasaki, M., Pietsch, W., Haberl, F., et al. 2012, *A&A*, 544, A144. doi:10.1051/0004-6361/201219025
- Sasaki, M., Haberl, F., Henze, M., et al. 2018, *A&A*, 620, A28. doi:10.1051/0004-6361/201833588
- Singh, K. P., Tandon, S. N., Agrawal, P. C., et al. 2014, *Proc. SPIE*, 9144, 91441S. doi:10.1117/12.2062667
- Stiele, H., Pietsch, W., Haberl, F., et al. 2011, *A&A*, 534, A55. doi:10.1051/0004-6361/201015270
- Sun, M., Jiang, B., Yuan, H., et al. 2021, *ApJS*, 254, 38. doi:10.3847/1538-4365/abf929
- Tandon, S. N., Subramaniam, A., Girish, V., et al. 2017, *AJ*, 154, 128. doi:10.3847/1538-3881/aa8451
- Tandon, S. N., Postma, J., Joseph, P., et al. 2020, *AJ*, 159, 158. doi:10.3847/1538-3881/ab72a3
- Truelove, J. K. & McKee, C. F. 1999, *ApJS*, 120, 299. doi:10.1086/313176
- Vancura, O., Blair, W. P., Long, K. S., et al. 1992, *ApJ*, 394, 158. doi:10.1086/171567
- Williams, B. F., Sjouerman, L. O., Kong, A. K. H., et al. 2004, *ApJ*, 615, 720. doi:10.1086/424589
- Williams, B. F., Lang, D., Dalcanton, J. J., et al. 2014, *ApJS*, 215, 9. doi:10.1088/0067-0049/215/1/9
- Yershov, V. N. 2014, *Ap&SS*, 354, 97. doi:10.1007/s10509-014-1944-5
- Yew, M., Filipović, M. D., Stupar, M., et al. 2021, *MNRAS*, 500, 2336. doi:10.1093/mnras/staa3382